Constraints on the tensor-to-scalar ratio for non-power-law models

Constraints on the tensor-to-scalar ratio for non-power-law models

J. Alberto Vázquez,[a,b] **M. Bridges,**[a,b] **Yin-Zhe Ma**[c,d] **and M.P. Hobson**[b]

[a]Kavli Institute for Cosmology,
  Madingley Road,Cambridge CB3 0HA, U.K.
[b]Astrophysics Group, Cavendish Laboratory,
  JJ Thomson Avenue, Cambridge, CB3 0HE, U.K.
[c]Department of Physics and Astronomy, University of British Columbia,
  Agricultural Road, Vancouver BC V6T 1Z1, Canada
[d]Canadian Institute for Theoretical Astrophysics, University of Toronto,
  St. George Street, Toronto Ontario M5S 3H8, Canada

  E-mail: jv292@cam.ac.uk, mb435@mrao.cam.ac.uk, mayinzhe@phas.ubc.ca,
  mph@mrao.cam.ac.uk

Abstract. Recent cosmological observations hint at a deviation from the simple power-law form of the primordial spectrum of curvature perturbations. In this paper we show that in the presence of a tensor component, a turn-over in the initial spectrum is preferred by current observations, and hence non-power-law models ought to be considered. For instance, for a power-law parameterisation with both a tensor component and running parameter, current data show a preference for a negative running at more than 2.5σ C.L. As a consequence of this deviation from a power-law, constraints on the tensor-to-scalar ratio r are slightly broader. We also present constraints on the inflationary parameters for a model-independent reconstruction and the Lasenby & Doran (LD) model. In particular, the constraints on the tensor-to-scalar ratio from the LD model are: $r_{\mathrm{LD}} = 0.11 \pm 0.024$. In addition to current data, we show expected constraints from Planck-like and CMB-Pol sensitivity experiments by using Markov-Chain-Monte-Carlo sampling chains. For all the models, we have included the Bayesian Evidence to perform a model selection analysis. The Bayes factor, using current observations, shows a strong preference for the LD model over the standard power-law parameterisation, and provides an insight into the accuracy of differentiating models through future surveys.

Contents

1 Introduction

Inflationary models have the merit that they not only explain the homogeneity of the universe on large-scales, but also provide a theory to explain the origin of perturbations as observed in the Cosmic Microwave Background (CMB). During the inflationary period, quantum fluctuations of the field were driven to scales much larger than the Hubble horizon and eventually turned into density perturbations (scalar) observed in the CMB and the large-scale distribution of galaxies, together with a gravitational wave (tensor) contribution. The vector contributions, however, are expected to be negligible since these modes decayed very rapidly once they entered the Hubble horizon. The scalar and tensor contributions are summarised by the primordial power spectrum $\mathcal{P}_{\mathcal{R}}(k)$ and $\mathcal{P}_{\mathcal{T}}(k)$, respectively. The scalar spectrum for a single-inflaton field ϕ, in the slow-roll approximation, is given by [22]:

$$\mathcal{P}_{\mathcal{R}}(k) = \left[\left(\frac{H}{\dot{\phi}} \right)^2 \left(\frac{H}{2\pi} \right)^2 \right]_{k=aH}, \tag{1.1}$$

where the expression is evaluated at the horizon exit $k = aH$. Since the initial spectrum is an unknown function, one needs to carry out a full numerical calculation from the onset of the inflationary phase, or to assume a particular functional form of it. The simplest proposal is to parameterise the shape of $\mathcal{P}_{\mathcal{R}}(k)$ by a power-law. Although the power-law assumption has provided reasonable agreement with cosmological observations, some recent analyses have shown that if a running of the scalar spectral-index is taken into account, there exists a preference for a negative running-value at 1.8σ C.L. from WMAP7+ACT (SPT) measurements [11, 16] and at 2.2σ C.L. with WMAP7+QUaD [4]. It has also been shown that the existence of a turn-over in $\mathcal{P}_{\mathcal{R}}(k)$, by using model-independent techniques, is preferred [14, 15, 24, 32]. The presence of this turn-over plays an important role in explaining current cosmological observations and cannot therefore be ignored when constraining the inflationary parameters. In the slow-roll approximation, the shape of the spectrum of tensor perturbations is

$$\mathcal{P}_{\mathcal{T}}(k) = \left[\frac{16}{\pi} H^2 \right]_{k=aH}, \tag{1.2}$$

which depends on the form of the scalar spectrum, and vice-versa, via the potential of the single scalar-field. To place constraints on the amplitude of tensor contributions, it is customary to define the tensor-to-scalar ratio as

$$r(k) \equiv \frac{\mathcal{P}_{\mathcal{T}}(k)}{\mathcal{P}_{\mathcal{R}}(k)} = 64\pi \left(\frac{\dot{\phi}^2}{H^2}\right)_{k=aH}. \tag{1.3}$$

The dependence of the scalar spectrum on the tensor spectrum is evident in the Lasenby & Doran model [19], where both spectra depend upon the same best-fit parameters. In a previous paper we found that standard ΛCDM models with a turn-over in the scalar spectrum are preferred over a simple power-law parameterisation [32]. In this work, by assuming a power-law parameterisation of the tensor spectrum, we show that the bending of the scalar spectrum is enhanced due to the presence of a tensor component. To avoid misleading results due to the particular choice of parameterisation, the shape of the scalar spectrum is described by employing a model-independent reconstruction. We then show that current constraints on the tensor-to-scalar ratio (1.3) are broadened for non-power law $\mathcal{P}_{\mathcal{R}}(k)$ models. We also discuss the constraints on r for a massive scalar-field in the Lasenby & Doran model. Finally, by considering future experiments we present their expected constraints on the inflationary parameters. For all the models, the Bayes factor is computed in order to perform a model comparison.

The paper is organised as follows: in the next section we list the data sets and the cosmological parameters considered. In section 3 we study different models suggested to describe the form of the scalar spectrum. Then, we show the resulting parameter constraints on the tensor-to-scalar ratio and the preferred form of the power spectrum using current cosmological observations. In the same section we provide future constraints on r expected by Planck-like and CMB-Pol experiments. Performance assumptions for Planck and CMB-Pol are taken from [26] and [2]. We present the model selection analysis in section 4, and our conclusions in section 5.

2 Theoretical framework

Even though the primary parameters in the standard ΛCDM model have already been tightly constrained and have little impact on the B-mode spectrum, it is worthwhile to perform a full parameter-space exploration to determine the tensor-to-scalar ratio constraints in each model. We assume purely Gaussian adiabatic scalar and tensor contributions in a flat ΛCDM model[1] specified by the standard parameters: the physical baryon $\Omega_{\rm b}h^2$ and cold dark matter density $\Omega_{\rm c}h^2$ relative to the critical density (h is the dimensionless Hubble parameter such that $H_0 = 100h \ {\rm kms^{-1}Mpc^{-1}}$), θ is $100\times$ the ratio of the sound horizon to angular diameter distance at last scattering surface, τ denotes the optical depth at reionisation. We consider the tensor-to-scalar ratio for each model i as $r_i = \mathcal{P}_{\mathcal{T}(i)}(k)/\mathcal{P}_{\mathcal{R}(i)}(k)$; hereafter we set $r_i = r_i(k_0)$ at a scale of $k_0 = 0.015{\rm Mpc^{-1}}$. A study of the appropriate scale to use is given by [9]. Aside from the Sunyaev-Zel'dovich (SZ) amplitude A_{SZ} used by WMAP analyses, the ACT likelihood incorporates two additional nuisance parameters: the total Poisson power A_p and the amplitude of the clustered power A_c. The parameters describing the primordial spectra for each model are listed in the next section, together with the flat priors imposed in our Bayesian analysis.

---

[1]Except for the LD model, which is based on a marginally closed universe $\Omega_k < 0$.
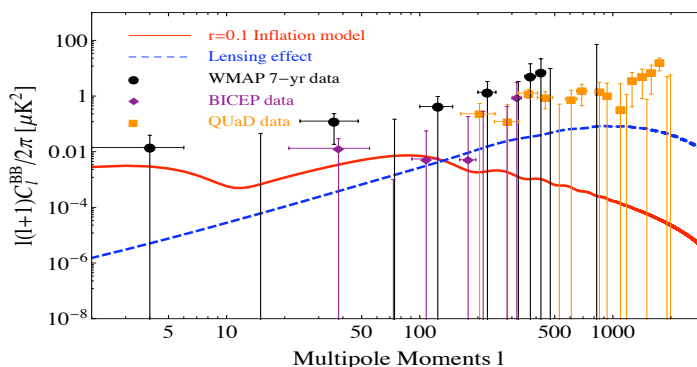
Figure 1. Comparison of theoretical prediction of $r = 0.1$ inflation model, and the WMAP, BICEP and QUaD data for the B-mode power spectrum.

Throughout the analysis, the theoretical temperature and polarisation C_ℓ's spectra are generated with a modified version of the CAMB code [21], and the parameter estimation is performed using the CosmoMC program [20]. The calculation of the Bayesian evidence $\mathcal{Z}$, to perform the model selection, requires a multidimensional integration over the likelihood and prior. To do this, we make use of the MULTINEST algorithm [12, 13]. The Bayes factor $\mathcal{B}_{ij}$, or equivalently the difference in log evidences $\ln \mathcal{Z}_i - \ln \mathcal{Z}_j$, provides a measure of how well model i fits the data compared to model j. In order to make a qualitative model comparison, we consider the Jeffreys guideline: if $\mathcal{B}_{ij} < 1$ model i should not be favoured over model j, $1 < \mathcal{B}_{ij} < 2.5$ constitutes significant evidence, $2.5 < \mathcal{B}_{ij} < 5$ is strong evidence, while $\mathcal{B}_{ij} > 5$ would be considered decisive [31, 33].

Current observations. To compute posterior probabilities for each model we use temperature and polarisation measurements from the Wilkinson Microwave Anisotropy Probe 7-year (WMAP7; [17]) and the Atacama Cosmology Telescope (ACT; [11]) data. To improve polarisation constraints, we include observations from QuaD [4], whose primary aim is high resolution measurements ($154 \leq \ell \leq 2026$) of the E-mode signal, and BICEP data [7] which probes intermediate scales ($21 \leq \ell \leq 335$). Figure 1 shows the B-mode spectrum predicted from a power-law parameterisation, with $r = 0.1$, along with 1σ constraints obtained by using current observations. In addition to CMB data, and to strengthen the constraining power, we incorporate distance measurements from the Supernova Cosmology Project Union 2 compilation (SCP; [1]) and Large Scale Structure data from the Sloan Digital Sky Survey (SDSS) Data Release 7 (DR7) Luminous Red Galaxy (LRG) power spectrum [29]. We also also consider baryon density information from Big Bang Nucleosyntesis (BBN, [6]) and impose a Gaussian prior on the Hubble parameter today H_0 from measurements of the Hubble Space Telescope (HST; [30]) key project.

Future surveys. In order to forecast expected constraints of future CMB observations, one can make use of the Fisher information matrix under the assumption that each parameter is Gaussian-distributed. However to obtain constraints more closely related to what is expected by future experiments, we perform a Monte Carlo analysis sampling over all variables involved in the description of the CMB spectrum. We simulate future experiments by generating mock
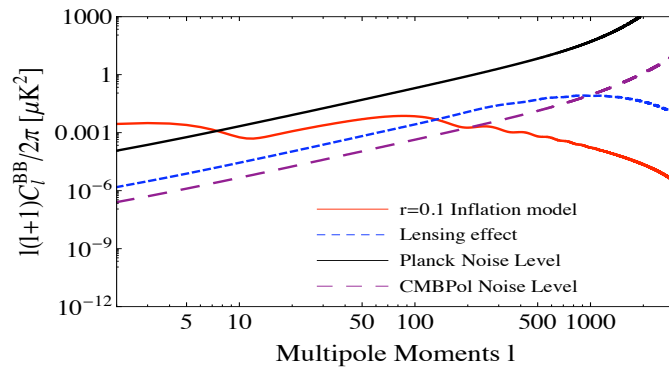
– 3 –

Figure 2. Polarization noise power spectra for forthcoming experiments. Note that these curves include uncertainties associated with the instrumental beam. The red line shows the B-mode power spectrum for the standard inflationary model with $r = 0.1$.

data of the $\hat{C}_\ell^{XY}$'s from a $\chi^2_{2\ell+1}$ distribution with variances [27]:

$$(\Delta \hat{C}_\ell^{XX})^2 = \frac{2}{(2\ell+1)f_{sky}} \left(C_\ell^{XX} + N_\ell^{XX} \right)^2, \tag{2.1}$$

$$(\Delta \hat{C}_\ell^{TE})^2 = \frac{2}{(2\ell+1)f_{sky}} \left[\left(C_\ell^{TE} \right)^2 + \left(C_\ell^{TT} + N_\ell^{TT} \right) \left(C_\ell^{EE} + N_\ell^{EE} \right) \right], \tag{2.2}$$

where $X = T, E$ and B label the temperature and polarisations; f_{sky} is the fraction of the observed sky. The C_ℓ^{XY}'s represent the theoretical spectra and N_ℓ^{XY} the instrumental noise spectra for each experiment. In experiments with multiple frequency channels c, the noise spectrum is approximated [3] by

$$N_\ell^X = \left(\sum_c \frac{1}{N_{\ell,c}^X} \right)^{-1}, \tag{2.3}$$

where the noise spectrum of an individual frequency channel, assuming a Gaussian beam, is

$$N_{\ell,c}^X = (\sigma_{\text{pix}} \theta_{\text{fwhm}})^2 \exp \left[\ell(\ell+1) \frac{\theta_{\text{fwhm}}^2}{8 \ln 2} \right] \delta_{XY}. \tag{2.4}$$

The pixel noise from temperature and polarisation maps are considered as uncorrelated. The noise per pixel σ_{pix}^X (and $\sigma_{\text{pix}}^P = \sqrt{2}\sigma_{\text{pix}}^T$) depends on the instrumental parameters; θ_{fwhm} is the full width at half maximum (FHWM) of the Gaussian beam.

For the Planck experiment, we include three channels with frequencies (100 GHz, 143 GHz, 217 GHz) and noise levels per beam $(\sigma_{\text{pix}}^T)^2$= (46.25 μK^2, 36 μK^2, 171 μK^2). The FHWM of the three channels are θ_{fwhm} =(9.5, 7.1, 5.0) arc-minute. These figures are taken from the values given in [26]. We combine three channels for the CMBPol experiment [2] with frequencies (100 GHz, 150 GHz, 220 GHz), noise levels $(\sigma_{\text{pix}}^T)^2 = (729$ nK^2, 676 nK^2, 1600 nK^2) and $\theta_{\text{fwhm}} = (8, 5, 3.5)$ arc-minute. Sky coverages of $f_{sky} = 0.65, 0.8$ are respectively assumed and integration time of 14 months. In figure 2 we show the noise levels for these experiments as a function of multipole number ℓ. The blue line corresponds to the B-mode power spectrum using the standard power-law parameterisation with $r = 0.1$. The lensed C_ℓ^B is also shown in the same figure, which can be treated as a part of the total noise power spectrum N_ℓ^B as well as the instrumental noise power spectra [25]. For more information of the noise and beam profile of each frequency channel please refer to [23].

3 Primordial power spectra constraints

3.1 Power-law parameterisation

Because slow-roll inflation predicts the spectrum of curvature perturbations to be close to scale-invariant, the simplest proposal is to assume that the initial spectrum has a power-law form, parameterised by

$$\mathcal{P}_{\mathcal{R}}(k) = A_s \left(\frac{k}{k_0} \right)^{n_s - 1}, \tag{3.1}$$

where the *spectral index* n_s is expected to be close to unity. A spectrum where the typical amplitude of perturbations is identical on all length scales is known as Harrison-Zel'dovich spectrum ($n_s = 1$), and it has been ruled out by several studies (see for instance [32]). Here, we assume, for simplicity, that the tensor spectrum is also described by a power-law function:

$$\mathcal{P}_{\mathcal{T}}(k) = A_t \left(\frac{k}{k_0} \right)^{n_t}, \tag{3.2}$$

where the tensor amplitude A_t is related to tensor-to-scalar ratio $r_s = A_t/A_s$. For this parameterisation we assume that $r(k_0)$ and the tensor spectral index $n_t \equiv d \ln \mathcal{P}_{\mathcal{T}}(k)/d \ln k$ satisfy the consistency relation for a single field slow-roll inflation $n_t = -r_s/8$ [10]. The power-law parameterisation thus contains only three free parameters: A_s, n_s, and r_s. For these parameters, we assume a prior $A_s = [1, 50] \times 10^{-10}$ for the amplitude, a conservative prior for the spectral index $n_s = [0.7, 1.2]$ and a tensor-to-scalar ratio prior of $r_s = [0, 1]$.

Figure 3 shows 1D and 2D marginalised posterior distributions of the scalar spectrum index n_s and the tensor-to-scalar ratio r_s, using both current cosmological observations (black line) and future experiments (red for Planck and green for CMBPol).

The bottom panel shows the limits imposed by current and future experiments. For present observations: $n_s = 0.964 \pm 0.011$ and $r_s < 0.171$ (mean values of 68% C.L. are quoted for two-tailed distributions, whilst one-tailed distribution only the upper 95% C.L.). These results are in agreement with previous studies, i.e. [11, 16, 17]. With regards to future constraints, we have used mean values obtained from current observations as the fiducial model (with fixed $r_s = 0.1$). We notice that 1σ error bars of the spectral index n_s, shown in the bottom panel of the same figure, reduce by about four times using a Planck-like experiment and five times for a CMBPol experiment. Whereas Planck will be able to distinguish tensor components with an accuracy of $\sigma_r = 0.013$, this is highly improved by CMBPol data $\sigma_r = 0.0009$. If we consider only one channel for comparison, e.g. 100 GHz, the constraints on the tensor-to-scalar ratio are given by $\sigma_r = 0.02$, in agreement with previous results [5]. The top-right panel of figure 3 illustrates the resulting shape of $\mathcal{P}_{\mathcal{R}}(k)$ corresponding to the posterior distributions using present data.

3.2 Running scalar spectral-index

A further extension is possible by allowing the scalar spectral index to vary as a function of scale, such that $n_s(k)$. This can be achieved by including a second order term in the expansion of the power spectrum

$$\mathcal{P}_{\mathcal{R}}(k) = A_s \left(\frac{k}{k_0} \right)^{n_s - 1 + (1/2) \ln(k/k_0)(dn/d \ln k)}, \tag{3.3}$$

$$(n_s)$$

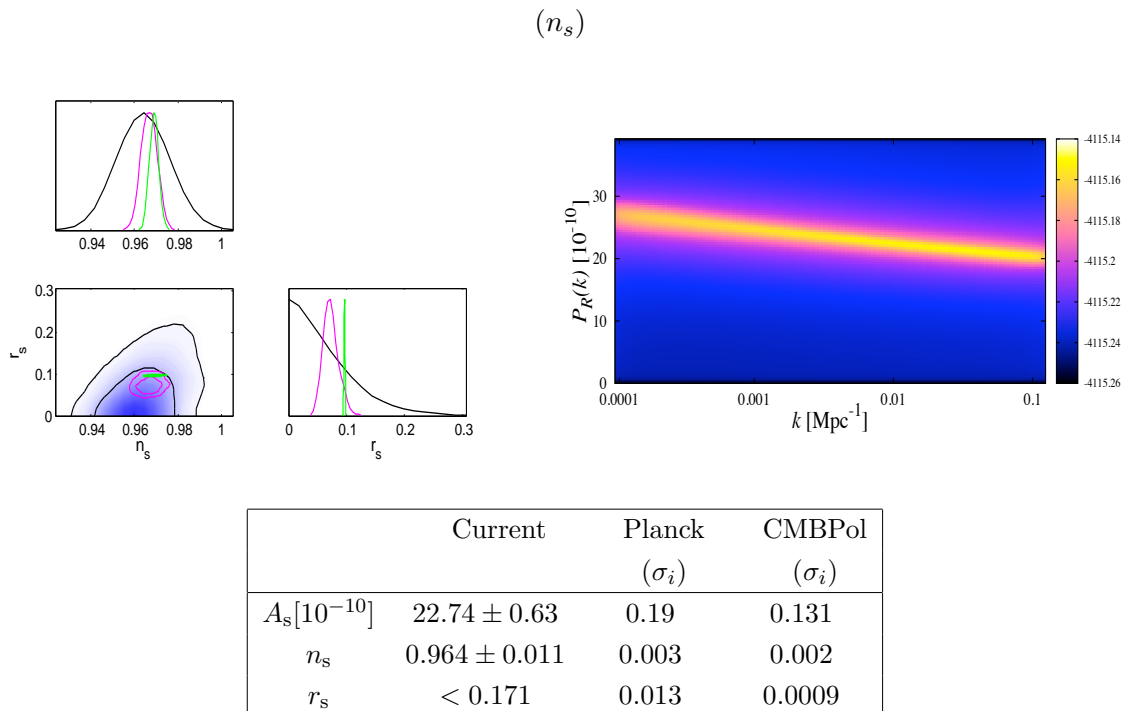|	Current	Planck	CMBPol
		(σ_i)	(σ_i)
$A_{\rm s}[10^{-10}]$	22.74 ± 0.63	0.19	0.131
$n_{\rm s}$	0.964 ± 0.011	0.003	0.002
$r_{\rm s}$	< 0.171	0.013	0.0009

Figure 3. Left panel: 1D and 2D probability posterior distributions for the power spectrum parameters, assuming a simple tilt parameterisation $(n_{\rm s})$; using both current observations (black line) and future experiments (red for Planck and green for CMBPol). 2D constraints are plotted with 1σ and 2σ confidence contours. Right panel: reconstruction of the scalar spectrum using present data; lighter regions represent an improved fit.

where $n_{\rm run} \equiv dn_{\rm s}/d\ln k$ is termed the *running of the tilt* and we would expect $n_{\rm run} \approx 0$ for standard inflationary models. We have kept the same tensor spectrum as in the simple power-law parameterisation, with a tensor-to-scalar ratio $r_{\rm run}$ at a scale of $k_0 = 0.015$ Mpc^{-1} to avoid correlations amongst parameters [9]. We maintained the same priors for the inflationary parameters $A_{\rm s}$, $n_{\rm s}$, and $r_{\rm run}$ and select a prior of the running parameter of $n_{\rm run} = [-0.1, 0.1]$ as used by [24].

Figure 4 shows the 1D and 2D marginalised posterior distributions for the inflationary parameters, using current experiments (black line): $n_{\rm s} = 0.985 \pm 0.017$, $n_{\rm run} = -0.043 \pm 0.018$ and $r_{\rm run} < 0.324$; and Planck (red line) and CMBPol (green line) realisations. The top label of the figure indicates the Bayes factor using present observations, which in this case and throughout the paper is compared with respect to the power-law parameterisation. We first note that in the presence of a tensor component the bending of the scalar spectrum is enhanced through a larger running parameter. That is because, at the largest scales, the contribution of the CMB-tensor spectrum compensates the power of the CMB-scalar, leaving hence the total CMB spectrum unaffected; for instance $n_{\rm run} = -0.043 \pm 0.018$ compared to $n_{\rm run} = -0.028 \pm 0.014$ without tensors. We also observe that using current experiments a negative $n_{\rm run}$ parameter in preferred by more than 2.5σ C.L. Hence the necessity to include a turn-over in the power spectrum. This result is confirmed by noticing the Bayes factor is significantly favoured compared to the simple power-law model, $\mathcal{B}_{n_{\rm run}, n_{\rm s}} = +2.0 \pm 0.3$. Considerations of the running of running of the spectral index are also being explored [28]. We notice that correlations created by the inclusion of the running parameter broaden the

$$(n_{\rm run})\ \mathcal{B}_{n_{\rm run},n_{\rm s}} = +2.0 \pm 0.3$$

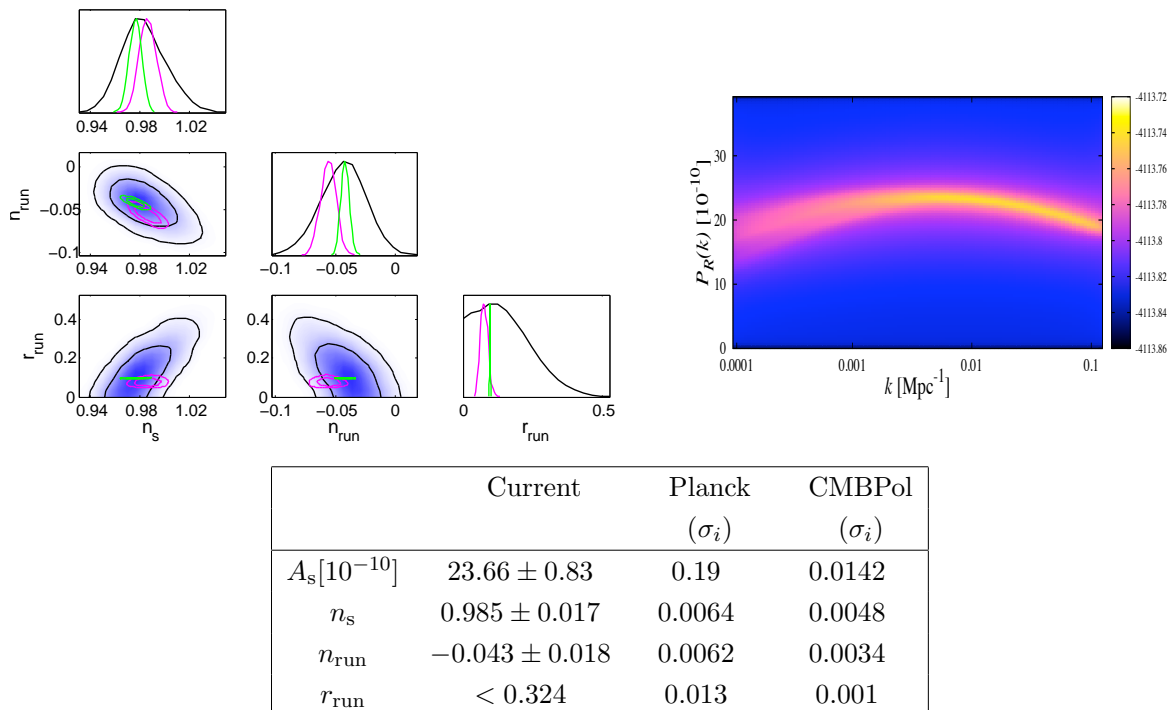|	Current	Planck (σ_i)	CMBPol (σ_i)
$A_{\rm s}[10^{-10}]$	23.66 ± 0.83	0.19	0.0142
$n_{\rm s}$	0.985 ± 0.017	0.0064	0.0048
$n_{\rm run}$	-0.043 ± 0.018	0.0062	0.0034
$r_{\rm run}$	< 0.324	0.013	0.001

Figure 4. Left panel: 1D and 2D probability posterior distributions for the inflationary parameters, assuming a power-law with a running parameter ($n_{\rm run}$); using both current data (black line) and future experiments (red for Planck and green for CMBPol). 2D constraints are plotted with 1σ and 2σ confidence contours. Right panel: Reconstruction of the scalar spectrum using present data; lighter regions represent an improved fit. The top label denotes the Bayes factor of the $n_{\rm run}$-model compared to the power-law $n_{\rm s}$-model, using current observations.

constraints on the tensor-to-scalar ratio by about 1.5 times. Future constraints are also broadened compared to the power-law parameterisation. The summary of the constraints on the inflationary parameters is shown in the bottom panel of figure 4, and the reconstruction of $\mathcal{P}_\mathcal{R}(k)$, using present data, in the top-right panel.

3.3 Model independent reconstruction

We have seen that deviations from the simple power-law, by the introduction of the running parameter, are relevant in explaining present data. In order to corroborate this result and look for deviations from the power-law parameterisation, we consider a model-independent reconstruction. The reconstruction process we follow is based on the approach used previously by [32]. We place two fixed k-nodes at sufficiently separated positions $[k_{\min}, k_{\max}]$, with varying amplitudes $[A_{{\rm s},k_{\min}}, A_{{\rm s},k_{\max}}]$, and place inside additional 'nodes' with the freedom to move around in both position k_i and amplitude $A_{{\rm s},k_i}$. We assume that most of the astrophysical information is encompassed within the scales $k_{\min} = 0.0001$ Mpc^{-1} and $k_{\max} = 0.3$ Mpc^{-1}. Outside of these limits we consider the spectrum to be constant with values equal to those at $k_{\min}$ and $k_{\max}$ respectively. We allow variations in the amplitudes with a conservative prior $A_{{\rm s},k_i} \in [1, 50] \times 10^{-10}$. To maintain continuity between k-nodes, a linear

interpolation is performed such that the form of the power spectrum is described by

$$\mathcal{P}_{\mathcal{R}}(k) = \begin{cases} A_{\text{s},k_{\min}} & k \leq k_{\min}, \\ A_{\text{s},k_i} & k_{\min} < k_i < k_{i+1} < k_{\max}, \\ A_{\text{s},k_{\max}} & k \geq k_{\max}, \end{cases} \tag{3.4}$$

and with linear interpolation for $\quad k_{\min} \leq k_i \leq k_{\max}$.

We have restricted the model-independent reconstruction to two internal-nodes which we consider are sufficient to provide an accurate description of the shape of the power spectrum. The tensor spectrum is parameterised by a power-law form, similarly to the one in section 3.1. Here the tensor-to-scalar ratio, given by $r_{2k_i} = A_t/P_{\mathcal{R}}(k_0)$, is computed at the scale $k_0 = 0.015 \text{ Mpc}^{-1}$ and also satisfies the consistency relation $r_{2k_i} = -n_t/8$; with prior $r_{2k_i} = [0,1]$.

The top-left panel of figure 5 displays the 1D and 2D marginalised posterior distributions for the parameters used in the model-independent reconstruction. At the largest scales, we observe the lack of tight constraints on the amplitude A_1, mainly due to the cosmic variance and correlations with other parameters. At smaller scales, the constraints on the amplitues (i.e. A_2, A_3 and A_4) get tighter. We notice the presence of a bi-modal distribution in the medium/small scales, represented by k_2, where the highest peak ($k \sim 0.01 \text{Mpc}^{-1}$) matches the position of the turn-over in the primordial spectrum, as seen in the top-right panel of figure 5. The other peak is located where the constraints seem to improve by updated data sets: at the overlapping of WMAP/ACT observations ($0.1 < k < 0.14$) with LRG7 measurements. The reconstructed spectrum clearly presents a turn-over, however with the bending at small scales less pronounced that in the running model. Notice that the Bayes factor, shown in the top label of the same figure, is significantly preferred over the simple tilt model, even though the two-internal-node reconstruction contains four additional parameters; it is also marginally preferred over the running model. Future experiments will be able to pin-down accurately the shape of the primordial spectrum at medium and small scales (k_2), however at the largest scales (k_1) the cosmic variance still dominates, as seen in the 1D posterior distribution of A_1. Current and future constraints of the inflationary parameters are summarised in the bottom panel of figure 5.

3.4 Lasenby & Doran model

The Lasenby & Doran model is based on the restriction of the total conformal time available in a closed universe [19]. At the largest scales, the predicted scalar and tensor spectra naturally incorporate a drop-off without the need to parameterise them, whilst, at small scales they mimic a slight running behaviour. An important point to bear in mind, is that in the LD model the functional forms of H and $\dot{\phi}$ during inflation are expressed using just two parameters b_0 and b_4 [32, 33]. These parameters describe the initial conditions, along with the standard cosmological parameters, and therefore the primordial spectra generated by the LD model are given in terms of

$$P_{\mathcal{R}}(k) = P_{\mathcal{R}}(k; b_0, b_4, \Omega_i, H_0), \qquad P_{\mathcal{T}}(k) = P_{\mathcal{T}}(k; b_0, b_4, \Omega_i, H_0). \tag{3.5}$$

Notice that the tensor-to-scalar ratio r_{LD} is a derived quantity in terms of the cosmological parameters, H_0, Ω_i, and the initial-conditions parameters b_0 and b_4:

$$r_{LD}(k) = r_{LD}(k; b_0, b_4, \Omega_i, H_0). \tag{3.6}$$

$(2\mathrm{k_i})\ \mathcal{B}_{2\mathrm{k_i},n_\mathrm{s}} = +2.3 \pm 0.3$

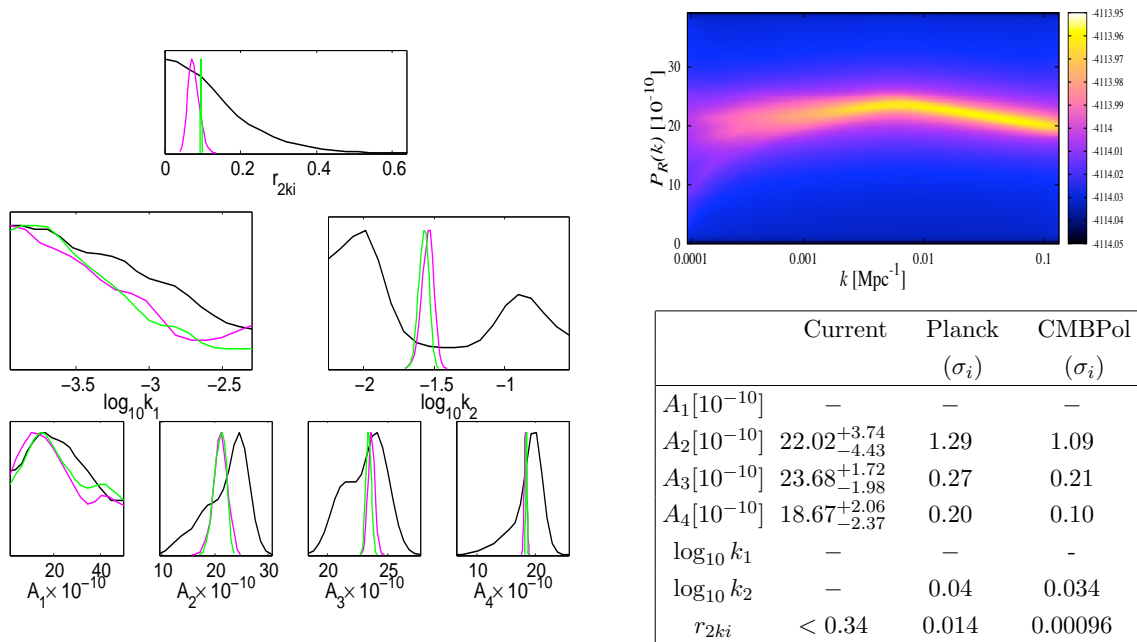|	Current	Planck	CMBPol
		(σ_i)	(σ_i)
$A_1[10^{-10}]$	–	–	–
$A_2[10^{-10}]$	$22.02^{+3.74}_{-4.43}$	1.29	1.09
$A_3[10^{-10}]$	$23.68^{+1.72}_{-1.98}$	0.27	0.21
$A_4[10^{-10}]$	$18.67^{+2.06}_{-2.37}$	0.20	0.10
$\log_{10} k_1$	–	–	-
$\log_{10} k_2$	–	0.04	0.034
r_{2ki}	< 0.34	0.014	0.00096

Figure 5. Left panel: 1D and 2D probability posterior distributions for the power spectrum parameters, assuming a two internal-node reconstruction $(2k_i)$; using both current cosmological observations (black line) and future experiments (red for Planck and green for CMBPol). 2D constraints are plotted with 1σ and 2σ confidence contours. Right panel: Reconstruction of the scalar spectrum using present data; lighter regions represents an improved fit. Top label denotes the Bayes factor of the $2k_i$-model compared to the power-law n_s-model, using current observations.

That is, if we use values of b_0 and b_4 along with the cosmological parameters there is no need to introduce additional variables to describe the tensor-to-scalar ratio r_{LD}. Figure 6 shows the primordial spectra, both scalar and tensor, for a given combination of b_0 and b_4 parameters. In the right panel of this figure, we illustrate the tensor-to-scalar ratio and its degeneracy with a selection of the parameters, for instance, the combination of $\{b_0 = 3.2, b_4 = -10 \times 10^{-10}\}$ or $\{b_0 = 3.0, b_4 = -12 \times 10^{-10}\}$ provides the same tensor-to-scalar ratio, even though their scalar and tensor spectra differ considerably. For further details about the LD model see, for instance [18, 19, 33]. To compute the LD spectra we refer to [32, 33]. We have also chosen the priors based on the same paper: $\Omega_k = [-0.05, 10^{-4}]$, $b_0 = [1, 4]$, $b_4 = [-30, -1] \times 10^{-9}$. Figure 7 shows 1D and 2D marginalised posterior distributions of the parameters involved in the description of the LD model. A novel result from the LD model is that its constraints on the tensor-to-scalar ratio are different from zero: $r_{\mathrm{LD}} = 0.11 \pm 0.024$, contrary to the standard power-law parameterisation. This happens mainly due to the ϕ^2-type potential assumed in the model.

The Bayes factor of this model compared to the simple-tilt model is shown in the top label of the same figure. The low number of parameters and the reduced power at both large and small scales make the LD model strongly favoured compared to the simple tilt and significantly so compared to the running and the two-internal-node reconstruction. Future experiments will provide an insight on discriminating amongst models, as we will see in the next section.
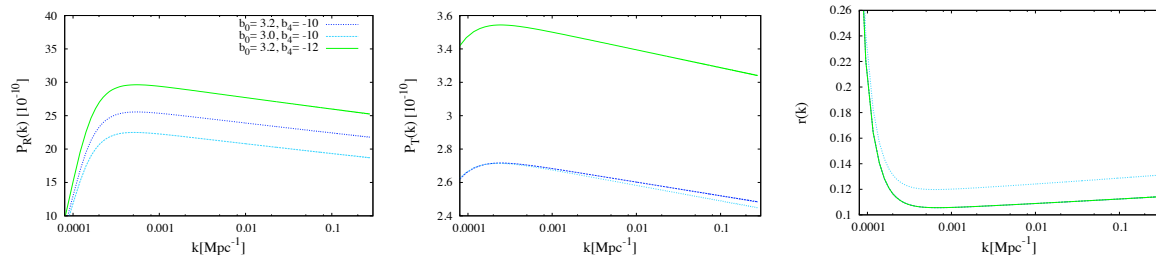
Figure 6. Derived primordial power spectra, $P_{\mathcal{R}}(k)$ and $P_{\mathcal{T}}(k)$, from the Lasenby & Doran model, using a different set of parameters of b_0 and b_4 (left and middle panels); units of b_4 are given in $[10^{-10}]$. The right panel shows the tensor-to-scalar ratio $r_{\mathrm{LD}} = P_{\mathcal{T}}/P_{\mathcal{R}}$.

(LD) $\mathcal{B}_{\mathrm{LD},n_s} = +3.4 \pm 0.3$

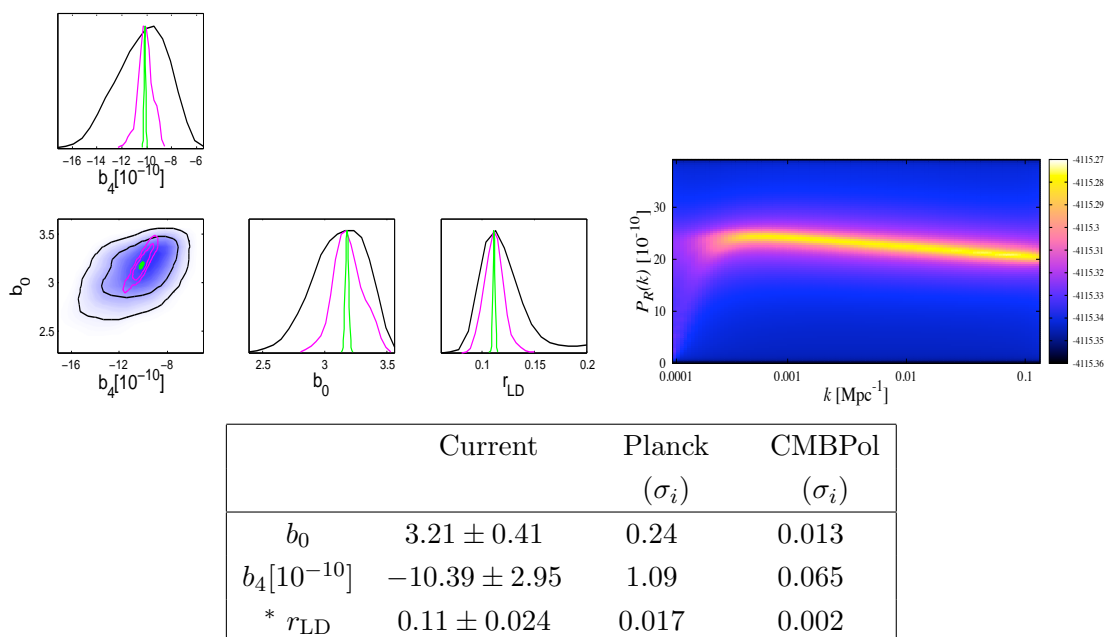|	Current	Planck	CMBPol
		(σ_i)	(σ_i)
b_0	3.21 ± 0.41	0.24	0.013
$b_4[10^{-10}]$	-10.39 ± 2.95	1.09	0.065
* r_{LD}	0.11 ± 0.024	0.017	0.002

Figure 7. 1D and 2D probability posterior distributions for the power spectrum parameters, assuming a Lasenby & Doran model (LD); using both current cosmological observations (black line) and future experiments (red for Planck and green for CMBPol). 2D constraints are plotted with 1σ and 2σ confidence contours. The top label denotes the associated Bayes factor with respect to the power-law n_s model using present data. *In this model, r_{LD} is a derived parameter.

4   Model selection

Throughout the analysis, we have included the Bayes factor for each model and found that the Lasenby & Doran model is the most preferred by current observations. Future experiments will be able to distinguish between models more effectively. Let us assume for a moment that the LD spectra represent the true model. We then use the LD spectra, with best-fit values obtained by using present data (shown in the bottom panel of figure 7), as the fiducial model to simulate future CMB observations. We analyse this mock data to reconstruct the input spectrum using the set of models aforementioned. Table 1 shows the Bayes factor for the different parameterisations compared to the LD model, along with the recovered tensor-to-

	Planck		CMBPol	
	$\mathcal{B}_{i,LD}$	r_i	$\mathcal{B}_{i,LD}$	r_i
LD	0.0 ± 0.3	0.102 ± 0.017	0.0 ± 0.3	0.100 ± 0.002
n_{s}	-6.3 ± 0.3	0.082 ± 0.014	-13.0 ± 0.3	0.105 ± 0.001
n_{run}	-6.5 ± 0.3	0.086 ± 0.015	-15.5 ± 0.3	0.103 ± 0.001
$2k_i$	-3.1 ± 0.3	0.091 ± 0.015	-10.2 ± 0.3	0.101 ± 0.001

Table 1. Model Selection. The input spectrum, given by the LD model, is reconstructed using different models. We show the Bayes factor for each model $\mathcal{B}_{i,LD}$, along with the recovered tensor-to-scalar ratio r_i.

scalar ratio. There is indeed a distinction between models, with the data clearly indicating a preference for the LD model, used to generate the input-simulated data. Idealised Planck results might provide decisive conclusions on distinguishing the LD model from the simple-tilt n_{s}-model, $\mathcal{B}_{n_s,LD} = -6.3 \pm 0.3$, and a running n_{run}-model, $\mathcal{B}_{n_{\mathrm{run}},LD} = -6.5 \pm 0.3$, and strong preference when compared to the two-internal-node reconstruction $2k_i$-model, $\mathcal{B}_{2k_i,LD} = -3.1 \pm 0.3$. There will also be a strong preference for the model independent reconstruction over both the n_{s} and n_{run} models: $\mathcal{B}_{2k_i,n_{\mathrm{s}}} = +3.2 \pm 0.3$ and $\mathcal{B}_{2k_i,n_{\mathrm{run}}} = +3.4 \pm 0.3$, respectively. With regards to the CMBPol experiment, this might definitely differentiate the LD spectrum from the rest of the spectra. In contrast to the Planck experiment, the model-independent reconstruction for CMBPol is now strongly favoured compared to the n_{run} model. CMBPol also provides a strong preference to differentiate the simple-tilt model n_{s} over the running model n_{run}: $\mathcal{B}_{n_{\mathrm{s}},n_{\mathrm{run}}} = +2.5 \pm 0.3$. Therefore, future experiments certainly will be able to differentiate between these models and pin down the right form of the primordial spectrum.

5 Discussion and conclusions

In this paper we have performed a MCMC exploration of the full cosmological parameter-space and showed current and future constraints on the inflationary parameters, with particular attention to the tensor-to-scalar ratio. We have considered models that deviate from the standard power-law in the scalar power-spectrum: a power-law parameterisation with running behaviour and the spectrum predicted from the Lasenby & Doran model. By implementing a model-independent reconstruction for $\mathcal{P}_{\mathcal{R}}(k)$, we found that a turn-over in the scalar spectrum is preferred to explaining cosmological observations. A similar form of the scalar spectrum has been previously obtained assuming different model-independent reconstructions, some of them with different data sets [14, 15, 32]. Even though we have not given the results for the standard cosmological parameters $\Omega_{\mathrm{b}}h^2$, $\Omega_{\mathrm{c}}h^2$, θ, τ, their best-fit values remained essentially unaffected throughout the models. For all the models, we have computed the Bayes factor and compared each to the simple power-law parameterisation. We found, using current observations, that the preferred model is given by the LD model. The summary of the analysis, illustrated in figure 8, displays how the constraints on the tensor-to-scalar ratio are broadened for non-power law models. We observe that the best-fit value of r_{run} is slighly offset from zero and coincides with the peak of r_{LD}. It has to be born in mind that if future surveys confirm small values of the true tensor-to-scalar ratio ($r \lesssim 0.09$), the LD model with a ϕ^2-type potential might be in conflict to reproduce this key feature. Throughout the models, the tensor-to-scalar ratio has been computed at a particular
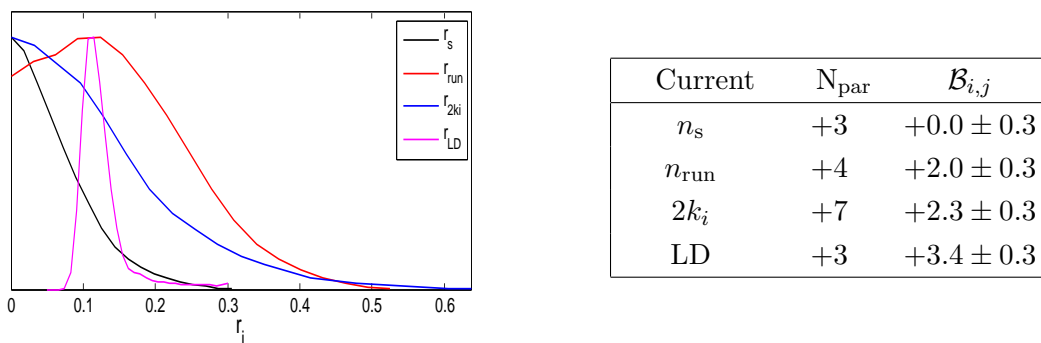
Figure 8. 1-D marginalised posterior distributions of the tensor-to-scalar ratio for the different models (left panel), along with their Bayesian evidence and number of parameters of each model (right panel). The Bayes factor is compared to the simple-tilt model ($n_{\rm s}$.)

scale $k_0 = 0.015$ Mpc^{-1}. However, to illustrate the robustness of the model selection, over a different choice of scale k_0, we compute the Bayesian evidence for all models at $k_0 = 0.002$ Mpc^{-1}. The results are esentially unaffected and still show a preference for the LD model. The Bayesian evidece, for each model, compared to the power-law parameterisation ($n_{\rm s}$) are as follow:

$$\mathcal{B}_{\rm run,n_s} \qquad \mathcal{B}_{\rm 2ki,n_s} \qquad \mathcal{B}_{\rm LD,n_s}$$
$$+1.8 \pm 0.3 \qquad +2.29 \pm 0.3 \qquad +3.0 \pm 0.3$$

We also notice that the tensor-spectrum in the LD model exhibits a running-like behaviour, contrary to the rest of the models. Nevertheless, the addition of a *running of the tilt* in the tensor modes, $n_{\rm run}^t \equiv d \ln n_t / d \ln k$, provides no significant changes to the Bayesian evidence. This can be seen from the fact that $n_{\rm run}^t$ is nearly zero, and also that no extra-parameters need to be included due to the existence of a second consistency relation: $n_{\rm run}^t \simeq n_t[n_t - (n_{\rm s}-1)]$ [8]. For instance, the Bayes factor of the $n_{\rm run}$-model with running in the tensor-spectrum is $\mathcal{B}_{n_{\rm run}+n_{\rm run}^t, n_{\rm run}} = +0.4 \pm 0.3$, with constraints $n_{\rm run}^t \times 1000 = 0.37 \pm 0.82$. A power-law parameterisation of $\mathcal{P}_{\mathcal{T}}(k)$ is therefore sufficient to describe current data. We will explore further possibilities in a more detailed future work.

With regards to future surveys, the Planck satellite will be able to differentiate the running and tilt model from the LD model, but not decisively from the two-internal-node reconstruction. The improvement using CMBPol selects the right form of the primordial spectrum, as shown in table 1.

Acknowledgments

References

[1] R. Amanullah, C. Lidman, D. Rubin, G. Aldering, P. Astier et al., *Spectra and Light Curves of Six Type Ia Supernovae at* $0.511 < z < 1.12$ *and the Union2 Compilation*, *Astrophys. J.* **716** (2010) 712 [arXiv:1004.1711] [INSPIRE].

[2] B-Pol collaboration, P. de Bernardis et al., *B-Pol: Detecting Primordial Gravitational Waves Generated During Inflation*, *Exper. Astron.* **23** (2009) 5 [arXiv:0808.1881] [INSPIRE].

[3] M. Bowden et al., *Scientific optimization of a ground-based CMB polarization experiment*, *Mon. Not. Roy. Astron. Soc.* **349** (2004) 321 [astro-ph/0309610] [INSPIRE].

[4] QUaD collaboration, M.L. Brown et al., *Improved measurements of the temperature and polarization of the CMB from QUaD*, *Astrophys. J.* **705** (2009) 978 [arXiv:0906.1003] [INSPIRE].

[5] C. Burigana et al., *Forecast for the Planck precision on the tensor to scalar ratio and other cosmological parameters*, *Astrophys. J.* **724** (2010) 588 [arXiv:1003.6108] [INSPIRE].

[6] S. Burles, K.M. Nollett and M.S. Turner, *Big bang nucleosynthesis predictions for precision cosmology*, *Astrophys. J.* **552** (2001) L1 [astro-ph/0010171] [INSPIRE].

[7] H. Chiang et al., *Measurement of CMB Polarization Power Spectra from Two Years of BICEP Data*, *Astrophys. J.* **711** (2010) 1123 [arXiv:0906.1181] [INSPIRE].

[8] M. Cortês and A.R. Liddle, *The consistency equation hierarchy in single-field inflation models*, *Phys. Rev.* **D 73** (2006) 083523 [astro-ph/0603016] [INSPIRE].

[9] M. Cortês, A.R. Liddle and P. Mukherjee, *On what scale should inflationary observables be constrained?*, *Phys. Rev.* **D 75** (2007) 083520 [astro-ph/0702170] [INSPIRE].

[10] M. Cortês, A.R. Liddle and D. Parkinson, *On the prior dependence of constraints on the tensor-to-scalar ratio*, *JCAP* **09** (2011) 027 [arXiv:1107.2673] [INSPIRE].

[11] J. Dunkley et al., *The Atacama Cosmology Telescope: Cosmological Parameters from the 2008 Power Spectra*, *Astrophys. J.* **739** (2011) 52 [arXiv:1009.0866] [INSPIRE].

[12] F. Feroz and M. Hobson, *Multimodal nested sampling: an efficient and robust alternative to MCMC methods for astronomical data analysis*, *Mon. Not. Roy. Astron. Soc.* **384** (2008) 449 [arXiv:0704.3704] [INSPIRE].

[13] F. Feroz, M. Hobson and M. Bridges, *MultiNest: an efficient and robust Bayesian inference tool for cosmology and particle physics*, *Mon. Not. Roy. Astron. Soc.* **398** (2009) 1601 [arXiv:0809.3437] [INSPIRE].

[14] Z.-K. Guo, D.J. Schwarz and Y.-Z. Zhang, *Reconstruction of the primordial power spectrum from CMB data*, *JCAP* **08** (2011) 031 [arXiv:1105.5916] [INSPIRE].

[15] Z.-K. Guo and Y.-Z. Zhang, *Uncorrelated estimates of the primordial power spectrum*, *JCAP* **11** (2011) 032 [arXiv:1109.0067] [INSPIRE].

[16] R. Keisler et al., *A Measurement of the Damping Tail of the Cosmic Microwave Background Power Spectrum with the South Pole Telescope*, *Astrophys. J.* **743** (2011) 28 [arXiv:1105.3182] [INSPIRE].

[17] WMAP collaboration, E. Komatsu et al., *Seven-Year Wilkinson Microwave Anisotropy Probe (WMAP) Observations: Cosmological Interpretation*, *Astrophys. J. Suppl.* **192** (2011) 18 [arXiv:1001.4538] [INSPIRE].

[18] A. Lasenby and C. Doran, *Conformal Models of de Sitter Space, Initial Conditions for Inflation and the CMB*, *AIP Conf. Proc.* **736** (2004) 53 [astro-ph/0411579] [INSPIRE].

[19] A. Lasenby and C. Doran, *Closed universes, de Sitter space and inflation*, *Phys. Rev.* **D 71** (2005) 063502 [astro-ph/0307311] [INSPIRE].

[20] A. Lewis and S. Bridle, *Cosmological parameters from CMB and other data: A Monte Carlo approach*, *Phys. Rev.* **D 66** (2002) 103511 [astro-ph/0205436] [INSPIRE].

[21] A. Lewis, A. Challinor and A. Lasenby, *Efficient computation of CMB anisotropies in closed FRW models*, *Astrophys. J.* **538** (2000) 473 [astro-ph/9911177] [INSPIRE].

[22] A.R. Liddle and D.H. Lyth, *COBE, gravitational waves, inflation and extended inflation*, *Phys. Lett.* **B 291** (1992) 391 [astro-ph/9208007] [INSPIRE].

[23] Y.-Z. Ma, W. Zhao and M.L. Brown, *Constraints on standard and non-standard early Universe models from CMB B-mode polarization*, *JCAP* **10** (2010) 007 [arXiv:1007.2396] [INSPIRE].

[24] D. Parkinson and A.R. Liddle, *Application of Bayesian model averaging to measurements of the primordial power spectrum*, *Phys. Rev.* **D 82** (2010) 103533 [arXiv:1009.1394] [INSPIRE].

[25] L. Perotto, J. Lesgourgues, S. Hannestad, H. Tu and Y.Y. Wong, *Probing cosmological parameters with the CMB: Forecasts from full Monte Carlo simulations*, *JCAP* **10** (2006) 013 [astro-ph/0606227] [INSPIRE].

[26] PLANCK collaboration, *The scientific programme of planck*, astro-ph/0604069 [INSPIRE].

[27] B.A. Powell, *Tensor Tilt from Primordial B-modes*, *Mon. Not. Roy. Astron. Soc.* **419** (2012) 566 [arXiv:1106.5059] [INSPIRE].

[28] B.A. Powell, *Scalar runnings and a test of slow roll from CMB distortions*, arXiv:1209.2024 [INSPIRE].

[29] B.A. Reid et al., *Cosmological Constraints from the Clustering of the Sloan Digital Sky Survey DR7 Luminous Red Galaxies*, *Mon. Not. Roy. Astron. Soc.* **404** (2010) 60 [arXiv:0907.1659] [INSPIRE].

[30] A.G. Riess et al., *A Redetermination of the Hubble Constant with the Hubble Space Telescope from a Differential Distance Ladder*, *Astrophys. J.* **699** (2009) 539 [arXiv:0905.0695] [INSPIRE].

[31] R. Trotta, *Bayes in the sky: Bayesian inference and model selection in cosmology*, *Contemp. Phys.* **49** (2008) 71 [arXiv:0803.4089] [INSPIRE].

[32] J.A. Vazquez, M. Bridges, M. Hobson and A. Lasenby, *Model selection applied to reconstruction of the Primordial Power Spectrum*, *JCAP* **06** (2012) 006 [arXiv:1203.1252] [INSPIRE].

[33] J.A. Vázquez, A. Lasenby, M. Bridges and M. Hobson, *A Bayesian study of the primordial power spectrum from a novel closed universe model*, *Mon. Not. Roy. Astron. Soc.* **422** (2012) 1948 [arXiv:1103.4619] [INSPIRE].